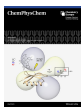

The Photocatalyzed Thiol-ene reaction: A New Tag to Yield Fast, Selective and reversible Paramagnetic Tagging of Proteins

Maxime Denis,[a, b] Charlotte Softley,[c, d] Stefano Giuntini,[b, e] Matteo Gentili,[a] Enrico Ravera,[e] Giacomo Parigi,[b, e] Marco Fragai,[b, e] Grzegorz Popowicz,[d] Michael Sattler,[c, d] Claudio Luchinat,[b, e] Linda Cerofolini,*[e] and Cristina Nativi*[b]

Paramagnetic restraints have been used in biomolecular NMR for the last three decades to elucidate and refine biomolecular structures, but also to characterize protein-ligand interactions. A common technique to generate such restraints in proteins, which do not naturally contain a (paramagnetic) metal, consists in the attachment to the protein of a lanthanide-binding-tag (LBT).

In order to design such LBTs, it is important to consider the efficiency and stability of the conjugation, the geometry of the complex (conformational exchanges and coordination) and the chemical inertness of the ligand. Here we describe a photocatalyzed thiol-ene reaction for the cysteine-selective paramagnetic tagging of proteins. As a model, we designed an LBT with a vinyl-pyridine moiety which was used to attach our tag to the protein GB1 in fast and irreversible fashion. Our tag **T1** yields magnetic susceptibility tensors of significant size with different lanthanides and has been characterized using NMR and relaxometry measurements.

1. Introduction

Nuclear magnetic resonance (NMR) is a powerful technique used for the study of biomacromolecules in solution. Indeed, it offers the opportunity to investigate structure, behavior, internal motions and mechanism of action of proteins, as well as their interactions with small molecules and other biomolecules at the atomic level.[1,2]

Structure calculation by NMR mainly relies on the collection of short-range distance restraints (up to ~5–6 Å) provided by the time-consuming and troublesome analysis of NOESY spectra. The use of long-range paramagnetic distance restraints (up to ~40 Å), such as pseudo-contact shifts (PCS), induced by a paramagnetic ion, has been widely proposed to help in *de novo* structure determination by NMR[3–8] or in the refinement of pre-existing X-ray structures.[9–11] In this way, a more reliable model describing the protein in solution can be obtained from the crystal structure .[12,13]

Furthermore, PCS restraints, together with residual dipolar coupling (RDC) restraints that originate from the same paramagnetic susceptibility tensor, have been exploited in the analysis of the internal dynamics of multi-domain proteins[14–21] and in the investigation of the interaction of proteins with their partners or ligands.[22–24]

One approach to incorporate paramagnetic metal ions into metallo-proteins is via the exchange of the naturally occurring diamagnetic metal ion.[25–27] As a more widely applicable alternative, any protein, not necessarily binding metal ions, can be made paramagnetic by attaching metal binding peptides or organic small synthetic ligands chelating paramagnetic metal ions.[28–33] The idea is to specifically attach the metal at a chosen position to monitor protein dynamics or protein-protein and protein-ligand interactions.[34]

To generate such restraints, one often relies on chemically synthesized lanthanide-binding tags (LBTs).[28] An important feature of LTBs is their ability to react quickly and selectively with a given amino acid in the protein. In addition, it is desirable that the metal coordination is rigid and avoids the presence of stereoisomers upon protein conjugation, which may complicate NMR data analysis. Apart from non-natural amino acids, paramagnetic tags generally target cysteines. The standard strategy is the conjugation by formation of a disulfide bond: this technique has been widely used but it is hampered

[a] *M.Sc. M. Denis, Dr. M. Gentili*
Giotto Biotech, S.R.L, Via Madonna del piano 6, 50019, Sesto Fiorentino (FI), Italy
[b] *M.Sc. M. Denis, Dr. S. Giuntini, Prof. G. Parigi, Prof. M. Fragai, Prof. C. Luchinat, Prof. C. Nativi*
Department of Chemistry "Ugo Schiff", University of Florence, Via della Lastruccia 3, 50019, Sesto Fiorentino (FI), Italy
E-mail: cristina.nativi@unifi.it
[c] *M.Sc. C. Softley, Prof. M. Sattler*
Biomolecular NMR, Department Chemie, Technical University of Munich, Lichtenbergstrasse 4, 85747, Garching, Germany
[d] *M.Sc. C. Softley, Dr. G. Popowicz, Prof. M. Sattler*
Institute of Structural Biology, Helmholtz Center Munich, Neuherberg, Germany
[e] *Dr. S. Giuntini, Dr. E. Ravera, Prof. G. Parigi, Prof. M. Fragai, Prof. C. Luchinat, Dr. L. Cerofolini*
Magnetic Resonance Center (CERM), University of Florence, and Consorzio Interuniversitario Risonanze Magnetiche di Metalloproteine (C.I.R.M.M.P), Via L. Sacconi 6, 50019 Sesto Florentino (FI), Italy
E-mail: cerofolini@cerm.unifi.it

Supporting information for this article is available on the WWW under https://doi.org/10.1002/cphc.202000071

by the stability of the bond formed.[35,36] Thus, in recent years, much effort has been concentrated on the design of paramagnetic tags that are stable under reducing conditions once attached to the protein,[37,38] and which could also be used in cells.[39] For this purpose, copper-catalyzed azide–alkyne "click" cycloadditions, (which, however, require the introduction of non-natural amino acids i.e. p-azido-phenylalanine[40] in the protein sequence), and thiol-ene coupling (TEC)[41] (which relies on existing or mutated cysteine residues) have emerged as useful alternative tools in protein chemical conjugation. In particular, thiol-ene coupling creates, through a radical mechanism, a stable thioether C–S bond between the free thiol of a cysteine and a double bonded carbon in an irreversible fashion. This reaction can be spontaneous but may also be photocatalyzed.[42] There are a few examples of the use of this reaction for the paramagnetic tagging of proteins[43] but the reactions are slow (overnight). Here, we describe a new vinyl-pyridine-based paramagnetic tag and its conjugation to proteins via the presented photo-catalyzed thiol-ene reaction to demonstrate that this reaction increases the applicability of paramagnetic tagging by making it suitable for proteins that are not stable for extended periods of time in vitro.

To design LBTs, it is important to consider the geometry of the complex and the chemical inertness of the ligand.[44] ((2S,2′S,2″S,2‴S)-1,1′,1″,1‴-(1,4,7,10-tetraazacyclododecane-1,4,7,10-tetrayl)tetrakis(propan-2-ol)), (S)-THP has been proposed as a simple yet enantiomerically pure[45] platform for the design of LBTs.[46] Hence, we have designed a THP-like LBT (**T1**) to be conjugated to proteins via TEC through a vinyl-pyridine group, as the single point of attachment.

We have tested the new tag with GB1 as a model protein with a single engineered cysteine residue. The effect of the designed LBT, chelating different paramagnetic metal ions (Lu^{3+}, Yb^{3+} and Dy^{3+}), on the resonances of the protein has been investigated by solution NMR. Relaxometry measurements were also performed to obtain information on the lanthanide coordination sites in **T1**(Ln).

2. Results and Discussion

2.1. Synthesis of T1

In order to synthesize **T1**, a picolinic-acid-like intermediate bearing the double-bond for conjugation and a leaving group for cyclen alkylation was needed. **A** was designated as a key intermediate in the synthesis. Derivative **A** was synthesized from commercial chelidamic acid (Figure 1). The carboxylic acids of chelidamic acid were protected as methyl esters and position 4 was brominated with tetrabutylammonium bromide (TBAB) and P_2O_5.

The reduction of a single methyl ester was easily achieved thanks to the peculiar reactivity of pyridine 2,6 diesters. The double bond in position 4 was then introduced via a Suzuki-like coupling[47] and the benzylic hydroxyl was subsequently replaced by a chloride as a good leaving group, giving **A** with a yield of 50% calculated over 5 steps.

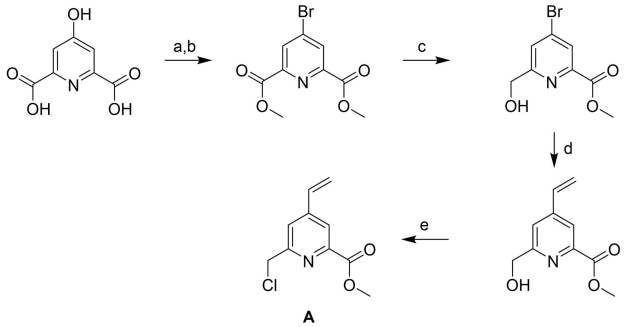

Figure 1. Synthesis of intermediate **A**
a. H_2SO_4, MeOH, 18 h, 98%. b. P_2O_5, TBAB, Tol, 3 h, 97%. c. $NaBH_4$, MeOH, 75% d. trivinyl-boroxin, K_3PO_4, JohnPhos, $Pd(dba)_2$, dioxane, 2 h, 68% e. MsCl, DIPEA, DCM, 95%

The intermediate **A** was then added to an excess of cyclen to isolate the mono functionalized cyclen derivative **B** (Figure 2). **B** was subsequently alkylated using (S)-propylene oxide and the methyl ester was deprotected to yield **C**. Lanthanide-chelation was achieved quantitatively, by refluxing overnight **C** in the presence of $LnCl_3$ salts in a H_2O/MeCN mixture.

2.2. Conjugation to GB1 T53C

In order to test our LBT we chose the GB1 T53C mutant as a model system. GB1 is a small globular protein which is stable under many conditions and was engineered to bear one cysteine. Vinyl picolinic acids have been shown to react through TEC with cysteines overnight by Su *et al.*,[43,48] but this reaction is quite slow (overnight). To reduce the reaction time, we used a photo-activated radical initiator, 2,2-dimethoxy-2-phenylacetophenone (DPAP), which has been shown to catalyze TEC when activated with UV at 365 nm.

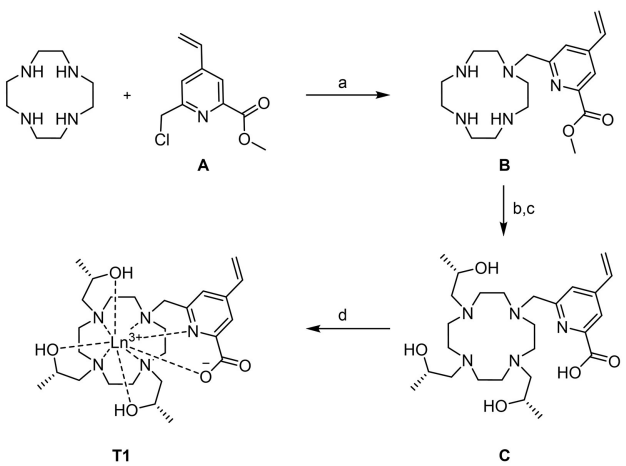

Figure 2. Synthesis of **T1**
a. DCM, 3 days b. (S)-propylene oxide, MeOH, 4 days, quant. c. LiOH, THF/H_2O, 18 h, quant. d. $LnCl_3$ nH_2O, H_2O/MeCN

To a solution of GB1, 5 equiv. of tag and 5 equiv. of DPAP were added. The mixture was irradiated by a UV lamp at 365 nm for 1 hour after which the sample was analyzed by NMR. We used **T1** loaded with Lu^{3+}, Yb^{3+} and Dy^{3+}. The protein tagging was evaluated recording 2D ^{1}H-^{15}N HSQC spectra which showed after 1 hour a conjugation of 80% (Figure 3). The reaction yield was evaluated from the relative intensity of the signals of free and conjugated protein. In each 2D ^{1}H-^{15}N HSQC, only one set of new peaks was observed, indicating that no side-reaction or protein degradation took place. We can assume that the reaction rate depends on the accessibility of the cysteine and on the stability of the corresponding thiyl species and may require protein-specific optimization. We can indeed expect that buried cysteines might not react under these conditions. For example, attempts to functionalize another protein, the small N-terminal domain of PEX14[49,50] were apparently hampered by the reduced solvent accessibility of the target cysteine on the protein surface and steric hindrance of the tag (see Supporting Information for more details). More radical initiator/UV wavelength couples could also be explored.

2.3. Evaluation of Paramagnetic Effects

The tagging of the T53C mono-cysteine variant of the GB1 protein with paramagnetic [**T1**(Yb)] and [**T1**(Dy)] resulted in PCS in the 2D ^{1}H–^{15}N HSQC spectrum (Figure 4). As expected, the

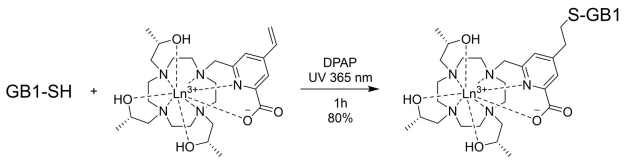

Figure 3. Tagging of GB1 with **T1** using the thiol-ene reaction.

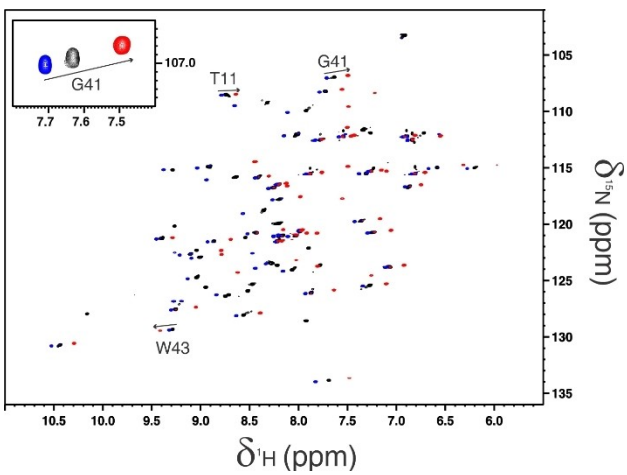

Figure 4. 2D ^{1}H–^{15}N HSQC of GB1 T53C tagged with [**T1**(Lu)] (black), [**T1**(Yb)] (blue) and [**T1**(Dy)] (red), acquired at 700 MHz and 298 K. In the insert, in the top-left corner, a zoom on residue G41 is shown. Interestingly, [**T1**(Yb)] and [**T1**(Dy)] provide shifts in the same directions for W43, because this residue is located at the interface between the negative and positive PCSs iso-surfaces.

two paramagnetic metal ions provide shifts in opposite directions.[25] In order to differentiate between the chemical shift perturbation stemming from the tagging itself and the paramagnetic contribution to the shifts (PCS), we also tagged GB1 with the diamagnetic [**T1**(Lu)]. The NMR signals, which shifted after the addition of the diamagnetic compound correspond to residues located close to the tagging-site (*c.f.* S.I. Figure S2). We note, that for each cross-peak in the 2D ^{1}H–^{15}N HSQC spectrum of diamagnetic samples only a single cross-peak is observed for the paramagnetic species. We therefore conclude that **T1** is indeed present as a single stereoisomer or a single conformation, giving rise to a single set of paramagnetically shifted peaks.

The PCS is described as a function of both the distance and orientation of the electron-nuclear spin vector and the magnitude of the anisotropy tensor ($\Delta\chi$),[51,52] according to the equation

$$\delta^{pc} = \frac{1}{12\pi r^3}\left[\Delta\chi_{ax}(3\cos^2\theta - 1) + \frac{3}{2}\Delta\chi_{rh}\sin^2\theta\cos 2\varphi\right]$$

where r, θ and φ are the spherical coordinates of the nucleus in the frame in which the anisotropy tensor is diagonal and has its origin at the metal position. $\Delta\chi_{ax}$ and $\Delta\chi_{rh}$ are the axial and rhombic components of the tensor, defined as

$$\Delta\chi_{ax} = \chi_{zz} - \frac{\chi_{xx} + \chi_{yy}}{2}$$

$$\Delta\chi_{rh} = \chi_{xx} - \chi_{yy}$$

The program FANTEN[53] was used to obtain the best fit $\Delta\chi$ tensor (consisting of 5 parameters: $\Delta\chi_{ax}$, $\Delta\chi_{rh}$, the three Euler angles defining the frame in which the tensor is diagonal) and the distance of the metal ion to the nuclear spins observed.

First, the resonances of 19 signals in the spectra of the protein tagged with [**T1**(Yb)] were unambiguously assigned, and the PCS were evaluated. The anisotropy tensor for the Yb^{3+} tagged protein was determined from the best fit of these 19 H^N PCS to the X-ray structure (PDB 1IGD),[54] using the program FANTEN. During these tensor calculations, the position of the metal was obtained. New NMR signals could then be assigned, taking advantage of the PCS values predicted by the program for the other nuclei, so that a total of 36 H^N PCSs were obtained for the [**T1**(Yb)] tagged protein.

The assignment of the spectrum of the protein tagged with [**T1**(Dy)] was obtained by comparison with the assigned spectra of the [**T1**(Yb)] and [**T1**(Lu)] tagged proteins (Figure 4); in this way 32 PCS were obtained for [**T1**(Dy)].

The PCS originating from [**T1**(Yb)] and [**T1**(Dy)] were first analyzed separately (Figure S3). The metal positions obtained from the two sets of data were similar (the metal is found at 8.6 and 8.1 Å, from the Cβ of the cysteine residue, for [**T1**(Dy)] and [**T1**(Yb)], respectively), as well as the direction of the main axes of the best fit tensors (Figure 5A and 5B).

Then, the two sets of PCSs were evaluated jointly by constraining both metals to reside in the same position. The

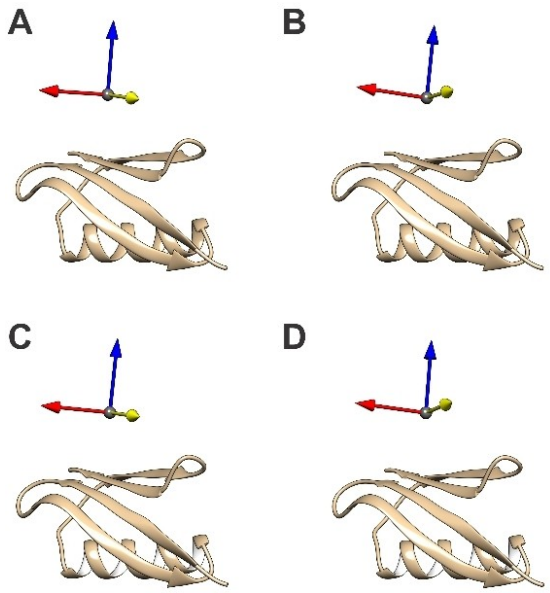

Figure 5. Graphical representation of the magnetic susceptibility anisotropy tensor orientations. The x, y and z axes (corresponding in turn to the directions with the smallest, intermediate and largest magnetic susceptibility) are represented as red, yellow and blue arrows, respectively. The panels A and C show the orientation of Yb tensors when only its own PCS dataset was considered, and when the datasets of Yb and Dy were both taken into account in FANTEN, respectively. The panels B and D show the orientation of the Dy tensors when only its PCS-data-set was considered, and when data sets of Yb and Dy where both taken into account in FANTEN, respectively.

Table 1. Tensor parameters calculated with the program FANTEN using the PCS values measured with [**T1**(Yb)] and [**T1**(Dy)] implemented separately or jointly in the evaluation of the metal position.

Metal	PCS source	Q factor	$\Delta\chi_{ax}$ (10^{-32} m^3)	$\Delta\chi_{rh}$ (10^{-32} m^3)
Yb	Yb	0.061	1.91 ± 0.02	0.68 ± 0.25
Dy	Dy	0.072	-6.51 ± 0.02	2.54 ± 0.89
Yb	Yb & Dy	0.064	1.83 ± 0.03	-0.59 ± 0.28
Dy	Yb & Dy	0.072	-6.81 ± 0.21	3.06 ± 0.89

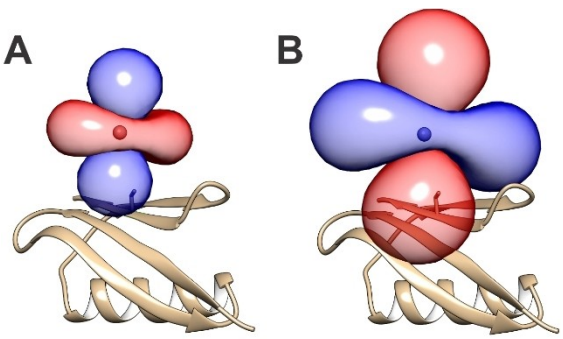

Figure 6. Graphical representation of PCS iso-surfaces of 1 (blue) and −1 (red) ppm obtained for [**T1**(Yb)] (A) and [**T1**(Dy)] (B) using the program FANTEN.

final position of the metal, obtained by FANTEN (8.3 Å from the Cβ of the cysteine residue), is very close to the positions found from the sets of data analyzed separately, and compatible with the expected covalent structure of the tag. The orientations and magnitudes of the two tensors were almost unaffected with respect to the values obtained from the separate fits, thus showing high consistency between the two sets of paramagnetic data (Table 1 and Figure 5). The two tensors are almost coaxial, with angles of 11.5° between the two Z-axes, 5° between the two X-axes and 12° between the two Y-axes.

The agreement between experimental and back-calculated PCS obtained from the fit of both sets of data is very good, with Q factors of 0.064 and 0.072, for [**T1**(Yb)] and [**T1**(Dy)], respectively (Figure S4). The PCS iso-surfaces for the two metals are represented in Figure 6.

It has been shown that some LBTs can be immobilized on the protein surface by an electrostatic interaction between the lanthanide cage and a carboxylate belonging to an Asp or Glu residue.[43,55] This interaction may decrease the tag mobility and therefore increase the magnitude of the magnetic susceptibility anisotropies. In the case of GB1 T53C, there are two carboxylates at distances of 9 and 11 Å from the cysteine (E42, E56), respectively. We therefore expected to see such a stabilizing interaction taking place between our tag and our protein. However, we find that the axial anisotropies of the two tensors are 4–5-fold reduced compared to the values expected for the anisotropies of the magnetic susceptibility tensors of the Yb^{3+} and Dy^{3+} ions usually calculated from rigid systems containing these paramagnetic ions.[56,57] This likely indicates that some motional averaging of the magnetic susceptibility tensors occurred, so that the best fit tensors result from the averaging of the magnetic susceptibility anisotropy tensors due to tag mobility.

Interestingly, the position of the metal calculated with FANTEN is relatively far from the protein surface. This observation corroborates the initial design of the tag to not interact with the protein surface, thus being very mobile, in agreement with the small tensor anisotropies observed. We suppose that in **T1** the lanthanide ions have a coordination number of 9 and have no further coordination site with which to interact with the carboxylate positioned on the protein surface.

The sizable mobility of the tag may be attributed to the two rotatable bonds, after the pyridine moiety, that tether the tag to the protein surface, which are absent in similar tags reported in the literature (such as DO3MA[58]). An additional methyl group on the pyridine moiety (i.e. in position 3 or 5) could have possibly restrained the rearrangement of the pyridine and stabilize the tag. Moreover, a different attachment site on the protein surface could have affected differently the tensor parameter values because of different possible protein/tag interaction (steric hindrance and/or hydrophobic interactions) which might rigidify the tag.

2.4. Relaxometry

To characterize the coordination of the lanthanides in **T1**, Fast Field Cycling (FFC) relaxometry experiments were performed.[59–62] The ^1H nuclear magnetic relaxation dispersion

(NMRD) profiles of the [**T1**(Gd)] complex in water solution at 10, 25 and 37 °C are shown in Figure 7. The profiles are characterized by dispersions somewhat smoother than predicted by the Lorentzian spectral density function; however, any attempt to reproduce them by considering inner sphere and outer-sphere contributions failed (with the diffusion coefficients constrained to values in the range expected for water solutions) unless the distance of closest approach between paramagnetic ion and diffusive water molecules was larger than 8 Å. Therefore, no sizable contribution from outer-sphere relaxation is apparent, and the profiles were fit by including two protons at a distance r_1 and other two protons at a distance r_2 from the Gd^{3+} ion (r_1 and r_2 were left free to be adjusted in the best fit analysis).

The best fit parameters are reported in Table 2 and the corresponding profiles are shown in Figure 7. Due to the low sensitivity to the correlation time τ_v for electron relaxation, the values of τ_v were kept fixed to values typically observed in gadolinium complexes.[63,64] Although there exists some covariance among the different parameters, the analysis indicates that the lifetime of the two protons at $r_1 = 3.05$ Å, $\tau_{M(1)}$, is as long as several microseconds (ca. 4 μs at 25 °C). The analysis also shows contributions from fast exchanging second-sphere water molecules, with a lifetime on the picosecond timescale. The number of these second-sphere water molecules is totally covariant with the metal-proton distance r_2; if one water molecule is considered, r_2 is about 3.5 Å.

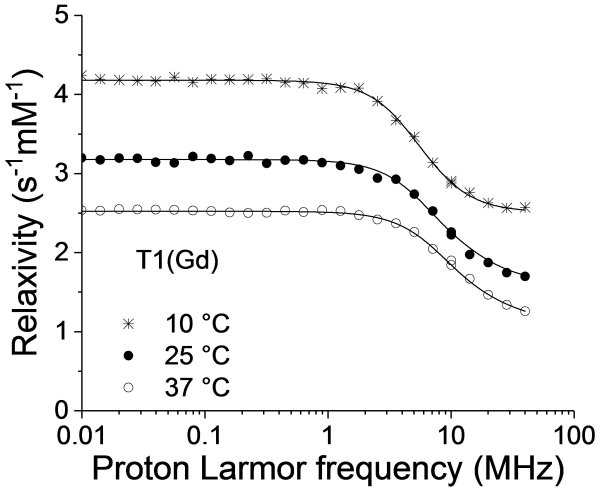

Figure 7. NMRD Profiles of [**T1**(Gd)] measured at different temperatures.

Table 2. Best fit parameters obtained from the NMRD profiles of [**T1**(Gd)], shown in Figure 7. Contributions from two protons in the first-coordination and second-coordination spheres were considered.

	37 °C	25 °C	10 °C
τ_R [ps]	35	57	112
Δ_t [cm^{-1}]	0.023		
τ_v [ps]	15	20	25
r_1 [Å]	3.05		
$\tau_{M(1)}$ [μs]	3.4	3.8	4.6
r_2 [Å]	3.48		
$\tau_{M(2)}$ [ps]	8.8	18	51

Fits of equivalent quality, however, can be obtained also for increasing values of r_1 (and decreasing values of r_2). When the condition $r_1 = r_2 = 3.3$ Å is met, almost indistinguishable best fit profiles are calculated, the complex reorientation time τ_R, the transient ZFS Δ_t and the lifetimes $\tau_{M(1)}$ and $\tau_{M(2)}$ being somewhat increased ($\tau_R = 84$ ps, $\Delta_t = 0.027$ cm^{-1}, $\tau_{M(1)} = 5.3$ μs and $\tau_{M(2)} = 28$ ps, at 25 °C).

The fast exchanging second-sphere water protons may be related to one or more water molecules hydrogen bonded in positions allowing for a large mobility.

The presence of two protons exchanging in the microsecond time scale at 3.05 Å, i.e. at the distance expected for the protons of a water molecule regularly coordinated to the Gd^{3+} ion, or at a somewhat larger distance (such as 3.3 Å), could be related to one water molecule hydrogen-bonded to the oxygen atoms of hydroxyl groups or of the carboxylate group. Its lifetime is much longer (several microseconds) than the lifetime of the water molecule coordinated to the Gd^{3+} ion in DO3A-like or DOTA-like complexes (on the sub-microsecond timescale), likely because of the bipositive charge of this complex which disfavours water exchange with respect to neutral or negative complexes.[65,66] A long lifetime of this water molecule indicates a relatively "compact" and stable environment surrounding the Gd^{3+} ion, which may prevent the replacement of the coordinated water by negatively charged groups present on the protein surface. This is in agreement with the observed tag mobility that affects the magnitude of the PCS-determined tensor. Alternatively, these slowly exchanging protons may be the hydrogen atoms of the three hydroxyl groups coordinated to the Gd^{3+} ion.

3. Conclusions

In this work, we present the synthesis and the performance of an enantiopure paramagnetic tag for NMR spectroscopy, designed to efficiently conjugate proteins under mild conditions using UV irradiation. In particular, we have demonstrated that UV-catalyzed TEC is applicable to the paramagnetic tagging of GB1 T53C with a high yield and short reaction times. The creation of the stable thioether bond required much shorter reactions times than previously described methods.[43,67]

The conjugation involves the protein's cysteine side-chain and forms thioether bonds without affecting the paramagnetic properties of the tag. Being easily obtained, and in high yields, the formation of non-reducible thioether bonds is convenient and makes this strategy a method of choice in the field of paramagnetic tagging, opening the way to development of more novel and rigid paramagnetic tags. Those tags could be applied to the study of larger systems, where the PCSs analysis could be complemented by the use of residual dipolar couplings and paramagnetic relaxation enhancements measurements.[68,69]

Experimental Section

Organic Synthesis

All the reagents were purchased from Sigma-Alrich, except cyclen which was purchased from Chematech. Small-molecules NMR experiments were recorded on a Bruker AVANCE II 500 MHz (^{1}H Larmor frequency) at 298 K. HPLC was performed with an Agilent 1200 Sries with ZORBAX 300SB-18 analytica and semi-preparative. Mass spectrometry was performed on a Thermo-Fisher LTQ-XL ESI.

Formation of Lanthanide Complexes

C (70 mg) and $LnCl_3$ nH_2O (100 mg) were dissolved in 6 mL H_2O/MeCN (50/50). The pH was adjusted to 7 and the mixture was refluxed. Chelation was typically quantitative overnight, as shown by LC/MS analysis. Reaction mixtures were purified via semi-preparative HPLC.

Protein Conjugation

GB1 T53C was expressed and purified as reported in the supplementary information. Prior to conjugation, the protein was buffer-exchanged into NaPi 20 mM, pH 7.5, then concentrated to 180 μM. 5 equivalents each of DPAP and [**T1**(Ln)] were added to the protein, as well as 10% D2O. The mixture was transferred into a 5-mm NMR tube and argon was gently bubbled through the solution for 5 minutes. The tube was placed under a UV Lamp (UVGL-55 Mineralight 26 W) at 365 nm for 1 h, after which the sample was measured using NMR spectroscopy and the spectra analyzed. Excess of small molecules were then washed away by buffer exchange and NMR spectra were recorded again.

NMR Measurements and PCS Analysis

All the experiments were acquired on a Bruker AVANCE NEO NMR spectrometer operating at 700 MHz (^{1}H Larmor frequency) at 298 K equipped with a 5 mm TCI 3 channels HCN cryo-probehead. All the spectra were processed with the Bruker TopSpin 4.0.7 software package and analysed with the program CARA[70] (ETH Zürich).

The spectra were collected using a protein concentration of ~180 μM in buffered solution (20 mM sodium phosphate pH 7.5).

The assignment of GB1 was taken from the literature.[71]

The PCS values were calculated from the difference in the value of chemical shift of each amino acid peak between the paramagnetic [**T1**(Yb) or **T1**(Dy)] and diamagnetic [**T1**(Lu)] 2D ^{1}H-^{15}N HSQC spectra acquired.

The fitting of the PCS tensor was carried out using the program FANTEN.[53]

Relaxometry Measuremnts

^{1}H nuclear magnetic relaxation dispersion (NMRD) profiles of the [**T1**(Gd)] complex in water solution were obtained by measuring the water proton relaxivity as a function of the applied magnetic field at the temperature of 10, 25 and 37 °C. The profiles were measured with a SPINMASTER2000 fast field cycling relaxometer (Stelar, Mede (PV), Italy) operating in the 0.01–40 MHz ^{1}H Larmor frequency range. The measurements are affected by an error below 1%, when fitted to a monoexponential decay/recovery of the magnetization in the field cycling experiment.

Acknowledgements

This worked received funding from the European Union's framework program for Research and Innovation Horizon 2020 (2014–2020) under the Marie–Slodowska Curie Grant agreement number 675555, Accelerated Early-staGe drug dIScovery (AEGIS). The authors also acknowledge the Fondazione Cassa di Risparmio di Firenze, the support of the University of Florence, the Recombinant Proteins JOYNLAB and Regione Toscana (CERM-TT and BioEnable); the support and the use of resources of Instruct-ERIC, a landmark ESFRI project, and specifically the CERM/CIRMMP Italy; the COST Action CA15209 (EURELAX) and iNEXT, Grant number 653706, funded by the Horizon 2020 program of the European Union.

Conflict of Interest

The authors declare no conflict of interest.

Keywords: biomolecular NMR · lanthanide coordination · paramagnetic tags · photocatalyzed thiol-ene reaction · protein structure refinement

[1] M. Nilges, P. R. L. Markwick, *PLoS Comput. Biol.* **2008**, *4*, DOI 10.1371/journal.pcbi.1000168.
[2] G. P. I. Bertini, K. S. McGreevy, *NMR of Biomolecules: Towards Mechanistic Systems Biology* **2012**.
[3] I. Bertini, A. Donaire, B. Jiménez, C. Luchinat, G. Parigi, M. Piccioli, L. Poggi, *J. Biomol. NMR* **2001**, *21*, 85–98.
[4] R. Barbieri, C. Luchinat, G. Parigi, *ChemPhysChem* **2004**, *5*, 797–806.
[5] G. Otting, *Annu. Rev. Biophys.* **2010**, *39*, 387–405.
[6] X. C. Su, B. Man, S. Beeren, H. Liang, S. Simonsen, C. Schmitz, T. Huber, B. A. Messerle, G. Otting, *J. Am. Chem. Soc.* **2008**, *130*, 10486–10487.
[7] A. Bahramzadeh, T. Huber, G. Otting, *Biochemistry* **2019**, *58*, 3243–3250.
[8] K. B. Pilla, G. Otting, T. Huber, *Structure* **2017**, *25*, 559–568.
[9] A. Carlon, E. Ravera, J. Hennig, G. Parigi, M. Sattler, C. Luchinat, *J. Am. Chem. Soc.* **2016**, *138*, 1601–1610.
[10] M. Rinaldelli, E. Ravera, V. Calderone, G. Parigi, G. N. Murshudov, C. Luchinat, *Acta Crystallogr. Sect. D, Biol. Crystallogr.* **2014**, *70*, 958–967.
[11] G. Pintacuda, M. John, X. C. Su, G. Otting, *Acc. Chem. Res.* **2007**, *40*, 206–212.
[12] A. Carlon, E. Ravera, G. Parigi, G. N. Murshudov, C. Luchinat, *J. Biomol. NMR* **2019**, *73*, 265–278.
[13] C. Nitsche, G. Otting, *Curr. Opin. Struct. Biol.* **2018**, *48*, 16–22.
[14] I. Bertini, L. Ferella, C. Luchinat, G. Parigi, M. V. Petoukhov, E. Ravera, A. Rosato, D. I. Svergun, *J. Biomol. NMR* **2012**, *53*, 271–280.
[15] E. Ravera, L. Sgheri, G. Parigi, C. Luchinat, *Phys. Chem. Chem. Phys.* **2016**, *18*, 5686–5701.
[16] L. Cerofolini, G. B. Fields, M. Fragai, C. F. G. C. Geraldes, C. Luchinat, G. Parigi, E. Ravera, D. I. Svergun, *J. Biol. Chem.* **2013**, *288*, 30659–30671.
[17] L. Russo, M. Maestre-Martinez, S. Wolff, S. Becker, C. Griesinger, *J. Am. Chem. Soc.* **2013**, *135*, 17111–17120.
[18] T. Saio, K. Ogura, H. Kumeta, Y. Kobashigawa, K. Shimizu, M. Yokochi, K. Kodama, H. Yamaguchi, H. Tsujishita, F. Inagaki, *Sci. Rep.* **2015**, *5*, 1–11.
[19] S. P. Skinner, W. M. Liu, Y. Hiruma, M. Timmer, A. Blok, M. A. S. Hass, M. Ubbink, *Proc. Natl. Acad. Sci. USA* **2015**, *112*, 9022–9027.
[20] E. H. Abdelkader, X. Yao, A. Feintuch, L. A. Adams, L. Aurelio, B. Graham, D. Goldfarb, G. Otting, *J. Biomol. NMR* **2016**, *64*, 39–51.
[21] J. L. Chen, Y. Yang, L. L. Zhang, H. Liang, T. Huber, X. C. Su, G. Otting, *Phys. Chem. Chem. Phys.* **2016**, *18*, 5850–5859.
[22] C. Nitsche, G. Otting, *Prog. Nucl. Magn. Reson. Spectrosc.* **2017**, *98–99*, 20–49.
[23] C. Tang, J. Iwahara, G. M. Clore, *Nature* **2006**, *444*, 383–386.
[24] L. De La Cruz, T. H. D. Nguyen, K. Ozawa, J. Shin, B. Graham, T. Huber, G. Otting, *J. Am. Chem. Soc.* **2011**, *133*, 19205–19215.

[25] I. Bertini, M. B. L. Janik, Y. Lee, C. Luchinat, A. Rosato, *J. Am. Chem. Soc.* **2001**, 4181–4188.
[26] L. Cerofolini, T. Staderini, S. Giuntini, E. Ravera, M. Fragai, G. Parigi, R. Pierattelli, C. Luchinat, *JBIC J. Biol. Inorg. Chem.* **2018**, *23*, 71–80.
[27] J. J. G. Moura, B. J. Goodfellow, I. C. N. Duarte Anjos, L. Macedo, B. F. Volkman, S. G. Nunes, I. Moura, J. L. Markley, *JBIC J. Biol. Inorg. Chem.* **2010**, *15*, 409–420.
[28] D. Joss, D. Häussinger, D. Joss, D. Häussinger, *Prog. Nucl. Magn. Reson. Spectrosc.* **2019**, DOI 10.1016/j.pnmrs.2019.08.002.
[29] D. Häussinger, J. R. Huang, S. Grzesiek, *J. Am. Chem. Soc.* **2009**, *131*, 14761–14767.
[30] P. H. J. Keizers, A. Saragliadis, Y. Hiruma, M. Overhand, M. Ubbink, *J. Am. Chem. Soc.* **2008**, *130*, 14802–14812.
[31] V. Baldoneschi, L. Cerofolini, E. Dragoni, A. Storai, C. Luchinat, M. Fragai, B. Richichi, C. Nativi, *ChemPlusChem* **2016**, *81*, 1333–1338.
[32] I. Bertini, V. Calderone, L. Cerofolini, M. Fragai, C. F. G. C. Geraldes, P. Hermann, C. Luchinat, G. Parigi, J. M. C. Teixeira, *FEBS Lett.* **2012**, *586*, 557–567.
[33] P. C. Luca Frullano, *Curr. Org. Synth.* **2011**, *8*, 535–565.
[34] P. H. J. Keizers, M. Ubbink, *Prog. Nucl. Magn. Reson. Spectrosc.* **2011**, *58*, 88–96.
[35] Q. Miao, W.-M. Liu, T. Kock, A. Blok, M. Timmer, M. Overhand, M. Ubbink, *Angew. Chem. Int. Ed.* **2019**, *58*, 13093–13100.
[36] X. C. Su, J. L. Chen, *Acc. Chem. Res.* **2019**, *52*, 1675–1686.
[37] T. Müntener, J. Kottelat, A. Huber, D. Häussinger, *Bioconjugate Chem.* **2018**, 1–46.
[38] F. Yang, X. Wang, B.-B. Pan, X.-C. Su, *Chem. Commun.* **2016**, *52*, 11535–11538.
[39] Y. Hikone, G. Hirai, M. Mishima, K. Inomata, T. Ikeya, S. Arai, M. Shirakawa, M. Sodeoka, Y. Ito, *J. Biomol. NMR* **2016**, *66*, 99–110.
[40] P. Widder, F. Berner, D. Summerer, M. Drescher, *ACS Chem. Biol.* **2019**, *14*, 839–844.
[41] A. Dondoni, A. Massi, P. Nanni, A. Roda, *Chem. Eur. J.* **2009**, *15*, 11444–11449.
[42] S. Staderini, A. Chambery, A. Marra, A. Dondoni, *Tetrahedron Lett.* **2012**, *53*, 702–704.
[43] Q.-F. Li, Y. Yang, A. Maleckis, G. Otting, X.-C. Su, *Chem. Commun.* **2012**, *48*, 2704.
[44] M. Devreux, C. Henoumont, F. Dioury, D. Stanicki, S. Boutry, L. Larbanoix, C. Ferroud, R. N. Muller, S. Laurent, *Eur. J. Inorg. Chem.* **2019**, 3354–3365.
[45] L. B. M. Lelli, G. Pintacuda, A. Cuzzola, *Chirality* **2005**, *211*, 201–211.
[46] M. D. Lee, C.-T. Loh, J. Shin, S. Chhabra, M. L. Dennis, G. Otting, J. D. Swarbrick, B. Graham, *Chem. Sci.* **2015**, *6*, 2614–2624.
[47] A. S. Norio Miyaura, *J. Chem. Soc. Chem. Commun.* **1979**, 866–867.
[48] F. H. Ma, J. L. Chen, Q. F. Li, H. H. Zuo, F. Huang, X. C. Su, *Chem. Asian J.* **2014**, *9*, 1808–1816.
[49] L. Emmanouilidis, M. Gopalswamy, D. M. Passon, M. Wilmanns, M. Sattler, *Biochim. Biophys. Acta Mol. Cell Res.* **2016**, *1863*, 804–813.
[50] M. Dawidowski, L. Emmanouilidis, V. C. Kalel, K. Tripsianes, K. Schorpp, K. Hadian, M. Kaiser, P. Mäser, M. Kolonko, S. Tanghe, A. Rodriguez, W. Schliebs, R. Erdmann, M. Sattler, G. M. Popowic, *Science (80-.).* **2017**, *355*, 1416–1420.
[51] G. Parigi, E. Ravera, C. Luchinat, *Prog. Nucl. Magn. Reson. Spectrosc.* **2019**, *114–115*, 211–236.
[52] D. Shishmarev, G. Otting, *J. Biomol. NMR* **2013**, *56*, 203–216.
[53] M. Rinaldelli, A. Carlon, E. Ravera, G. Parigi, C. Luchinat, *J. Biomol. NMR* **2015**, 21–34.
[54] D. B. W. J. P. Derrick, *J. Mol. Biol.* **1994**, *243*, 906–918.
[55] K. L. Gempf, S. J. Butler, A. M. Funk, D. Parker, *Chem. Commun.* **2013**, 9104–9106.
[56] S. Dasgupta, X. Hu, P. H. J. Keizers, W. M. Liu, C. Luchinat, M. Nagulapalli, M. Overhand, G. Parigi, L. Sgheri, M. Ubbink, *J. Biomol. NMR* **2011**, *51*, 253–263.
[57] E. Ravera, G. Parigi, C. Luchinat, *J. Magn. Reson.* **2019**, *306*, 173–179.
[58] F. Yang, X. Wang, B. Bin Pan, X. C. Su, *Chem. Commun.* **2016**, *52*, 11535–11538.
[59] M. Fragai, E. Ravera, F. Tedoldi, C. Luchinat, G. Parigi, *ChemPhysChem* **2019**, *20*, 2204–2209.
[60] V. C. Pierre, M. Botta, S. Aime, K. N. Raymond, *J. Am. Chem. Soc.* **2006**, *128*, 5344–5345.
[61] L. Granato, L. Vander Elst, C. Henoumont, R. N. Muller, S. Laurent, *Chem. Biodiversity* **2018**, *15*, DOI 10.1002/cbdv.201700487.
[62] S. Aime, M. Botta, D. Esteban-Gómez, C. Platas-Iglesias, *Mol. Phys.* **2019**, *117*, 898–909.
[63] L. M. Lilley, K. Du, M. D. Krzyaniak, G. Parigi, C. Luchinat, T. D. Harris, T. J. Meade, *Inorg. Chem.* **2018**, *57*, 5810–5819.
[64] P. Caravan, J. J. Ellison, T. J. McMurry, R. B. Lauffer, *Chem. Rev.* **1999**, *99*, 2293–2352.
[65] A. E. M. É. Tóth, L. Burai, E. Brücher, *J. Chem. Soc. Dalton Trans.* **1997**, 1587–1594.
[66] S. Aime, A. Barge, M. Botta, D. Parker, A. S. De Sousa, *J. Am. Chem. Soc.* **1997**, *119*, 4767–4768.
[67] Y. Yang, J.-T. Wang, Y.-Y. Pei, X.-C. Su, *Chem. Commun.* **2015**, *51*, 2824–2827.
[68] W. Andrałojć, Y. Hiruma, W. M. Liu, E. Ravera, M. Nojiri, G. Parigi, C. Luchinat, M. Ubbink, *Proc. Natl. Acad. Sci. USA* **2017**, *114*, E1840–E1847.
[69] G. M. Clore, C. Tang, J. Iwahara, *Curr. Opin. Struct. Biol.* **2007**, *17*, 603–616.
[70] Rochus L. J. Keller, *The Computer Aided Resonance Assignment Tutorial (CARA)*, CANTINA Verlag, Goldau **2004**.
[71] D. J. Wilton, R. B. Tunnicliffe, Y. O. Kamatari, K. Akasaka, M. P. Williamson, *Proteins* **2007**, 1432–1440.

Manuscript received: January 27, 2020
Revised manuscript received: February 21, 2020
Accepted manuscript online: February 24, 2020
Version of record online: March 19, 2020